Production and Properties of Highly Oriented Polypropylene by Die Drawing

A. K. TARAIYA, A. RICHARDSON, and I. M. WARD, *Department of Physics, University of Leeds, Leeds LS2 9JT, England*

Synopsis

A comprehensive examination of the die-drawing behavior of polypropylene has been carried out, examining the effects of draw temperature, haul-off speed, and initial billet size. A range of oriented products was obtained and characterized, primarily by the determination of Young's modulus at room temperature, the maximum modulus being 20 GPa for a draw ratio R_A of 23.2. Using a large-scale machine, it was found possible to produce drawn products at speeds up to 2 m min^{-1} at a draw temperature of 155°C and R_A of 19.3. The dynamic mechanical behavior of several drawn materials was studied over the temperature range −80 to +80°C. It was of particular interest that the β relaxation was found to be absent in samples of high draw ratio.

INTRODUCTION

In recent years there have been numerous studies of the solid-phase deformation of polymers as a method for producing high-stiffness materials. Solid-state deformation in polymers can be produced by a number of processes. Some major techniques are tensile drawing,[1-5] hydrostatic extrusion,[6-12] ram extrusion,[13-18] and, more recently, die drawing.[19-28]

Die drawing is a technique that combines the best features of free tensile drawing and solid-state extrusion, enabling large-section products to be made at the high modulus levels obtainable by free drawing. The die drawing process developed in this laboratory[19,20] is shown schematically in Figure 1. A heated polymer billet is drawn through a heated conical die by applying a pulling force on the billet at the exit side of the die. The polymer billet is free to neck down and follows an optimum strain and strain rate path through the die, leaving the die wall at an appropriate point and hence considerably reducing the required flow stress.

Deformation can be considered to take place in three distinct zones, as shown in Figure 1, which can be briefly described as follows:

Zone 1. Isothermal conical die flow; in this region the material billet remains in contact with the die.

Zone 2. Free tensile isothermal flow; in this region the material necks down free of the die wall but should remain substantially at the die temperature.

Zone 3. In this region the material necks down further beyond the die under nonisothermal conditions.

The material progressively cools in zone 3, and deformation ceases at some point after the die, the cross-sectional area of the product then remaining constant.

Journal of Applied Polymer Science, Vol. 33, 2559–2579 (1987)

CCC 0021-8995/87/072559-21$04.00

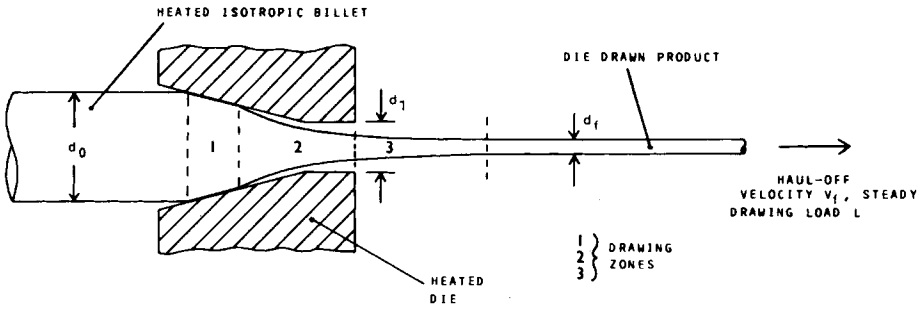

Fig. 1. Schematic diagram of the die drawing process.

The degree of deformation imparted to the material by the die drawing process is characterized by the actual draw ratio R_A, which is expressed in terms of the initial and final cross-sectional dimensions of the product:

$$R_A = \frac{\text{initial billet cross-sectional area}}{\text{final product cross-sectional area}}$$

For circular cross-sectional rods,

$$R_A = \left(\frac{d_0}{d_f}\right)^2$$

where: d_0 = billet diameter
d_f = final product diameter.

The initial billet size is characterized by R_N, the nominal deformation ratio, which is defined as the ratio of the billet cross-sectional area to that of the die exit:

$$R_N = \left(\frac{d_0}{d_1}\right)^2$$

where d_1 = die exit diameter.

The actual deformation ratio is always greater than the nominal deformation ratio since the polymer draws away from the die wall during the process.

Under stable die drawing conditions, the true draw stress at any point along the drawing path is a function of deformation ratio R at any point and is given by

$$\sigma_{\max} = \frac{4LR}{\pi d_0^2}$$

where L is steady haul-off load.

The maximum draw stress $\sigma_{\max}$ is expressed at and beyond the limit of deformation where zone 3 ends and is given by

$$\sigma_{\max} = \frac{4LR_A}{\pi d_0^2} = \frac{4L}{\pi d_f^2}$$

Many materials have been die drawn in this laboratory, including linear polyethylene (LPE),[20,21,28] polypropylene (PP),[19] polyoxymethylene (POM),[22] poly(vinylidene fluoride) (PVDF),[24] and poly(aryl ether ketone) (PEEK).[25]

EXPERIMENTAL

Materials and Billet Preparation

The material investigated in this study was a polypropylene copolymer, Propathene grade GSE 108 (melt flow index = 0.8) manufactured by I.C.I. plc and supplied in bar stock form.

Each billet was machined to the required diameter d_0 for die drawing at a given nominal draw ratio R_N. A tapered cone was turned on each billet with a tag of 4.0 mm diameter and 20 mm length to allow gripping and to assist the start-up procedure for the process. The length of each billet was about 150 mm.

Die Drawing Apparatus

The majority of the die drawing was performed with equipment designed for use on an Instron tensile testing machine. This die drawing apparatus is shown in Figure 2.

A conical steel die of semiangle 15° was used, the bore diameter at the exit and the land length both being 4.0 mm. The die drawing apparatus and start-up procedure have been described in detail earlier.[19-25]

A continuously variable haul-off speed from 5 to 500 mm min^{-1} was available on the Instron machine by use of the appropriate crosshead controls.

In order to investigate the effect of draw speed on the deformation ratio attained and the draw load, it was appropriate to increase draw speed V_f several times during each run. Following an increase in V_f, the load generally rose quite steadily until a new stable load was reached, corresponding to a different set of steady-state conditions. This procedure was repeated until a limiting draw speed was reached at which the product fractured, or up to the maximum limiting speed allowed on the Instron machine, for each nominal billet size R_N.

Large-scale Die Drawing

The small-scale die drawing apparatus mounted on the Instron was limited to a speed of 500 mm min^{-1}, and the product length was restricted by the crosshead travel limits. In order to draw the material at a faster rate, a large-scale die drawing machine was used. This machine was designed and constructed in this laboratory and is described in detail elsewhere.[28] The maximum geared draw speed was 2000 mm min^{-1}, and a draw travel length of 11 m was available.

The same die of 4.0 mm exit diameter as previously used was mounted via an adapter in the heating chamber of this equipment.

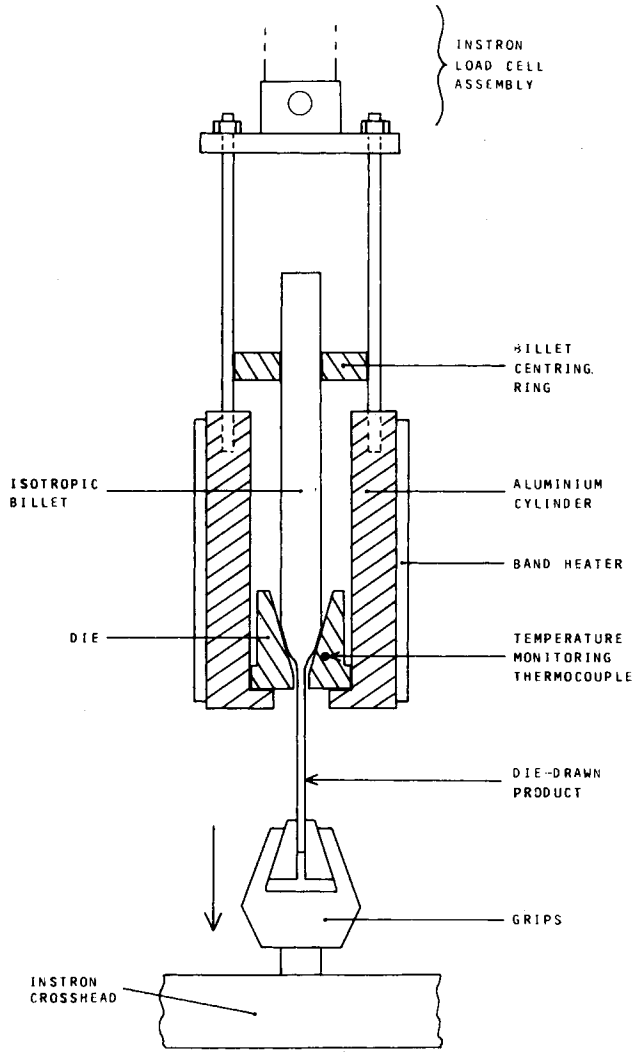

Fig. 2. Small-scale die drawing assembly.

Stiffness Measurements

A dead loading static three-point bend test apparatus was used at 20°C to measure the product isochronous (10 s) Young's modulus. A maximum strain of 10^{-3} was imposed, and high sample aspect ratios were maintained to minimize end effects.

Dynamic Mechanical Testing

The in-phase dynamic modulus E' and the loss factors $\tan \delta$ were measured in the three-point bending mode for the rods at a frequency of 1.69 Hz. The apparatus and technique are described comprehensively elsewhere.[29]

The test sample was enclosed in an insulated chamber in which the temperature could be varied between -80 and $+80$°C by cooled and heated

nitrogen streams. Measurements were taken on reheating after each sample had been slowly cooled to −80°C, the average heating rate then being 0.5°C min^{-1}.

RESULTS AND DISCUSSION

Processing Behavior

Die drawing of polypropylene grade GSE 108 at a draw temperature of 110°C on billet sizes of $R_N = 5$ and 7 was studied earlier in this laboratory.[19] In the present comprehensive examination of the die drawing behavior of polypropylene, a selection of billet R_N sizes was drawn at different temperatures over a wide range of haul-off speeds. The results are shown in Figure 3, where the most apparent feature is the increase in draw ratio with increasing draw speed. The maximum draw speed was limited by product fracture in certain cases or by machine drawing speed (500 mm min^{-1}) in others. If fracture occurred, this followed the formation of a localized neck in the

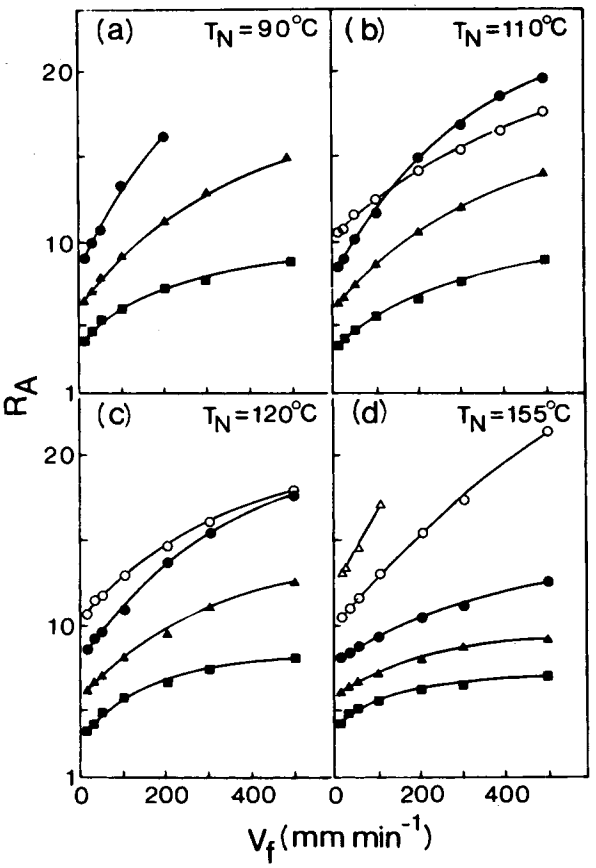

Fig. 3. Variation of draw ratio R_A with draw speed V_f, draw temperatures as indicated: ■ $R_N = 3$; ▲ $R_N = 5$; ● $R_N = 7$; ○ $R_N = 9$; △ $R_N = 11$.

product, just beyond the die exit, and was usually preceded by stress whitening of that necked region.

At $T_N = 90°C$ (Fig. 3a), $R_N = 3$ and 5 billets were drawn at up to 500 mm min^{-1} without fracture. Maximum draw ratios of 8.7 and 14.7 were obtained for the $R_N = 3$ and 5 billets, respectively, at this draw speed. Billets of $R_N = 7$ were drawn up to a draw speed of 200 mm min^{-1}, beyond which fracture occurred; a maximum draw ratio of 16.2 was achieved. Early fracture was observed for $R_N = 9$ billets at the start-up phase.

At $T_N = 110°C$ (Fig. 3b), billets of $R_N = 3$ and 5 were drawn successfully up to the maximum machine speed; the maximum draw ratios obtained were 8.9 and 14.0, respectively. At this temperature it was found possible to draw $R_N = 7$ billets up to speeds of 500 mm min^{-1} without fracture, at which a maximum draw ratio of 19.5 was obtained. $R_N = 9$ billets could also be drawn, the draw ratios obtained being lower than the draw ratios at $R_N = 7$ for draw speeds higher than 130 mm min^{-1}. Stress whitening in the $R_N = 9$ products was observed, and at higher draw speeds, surface material disruption also occurred. The apparent low R_A values for $R_N = 9$ may be due to overestimates of diameter and hence cross-section area due to surface disruption. It would therefore appear that for $R_N = 9$ billets the draw temperature was too low for drawing of a smooth-surfaced product, high stresses in the material occurring, as will be discussed later. However, it was possible to draw $R_N = 9$ billets up to speeds of 500 mm min^{-1}, at which the maximum draw ratio was 17.5.

At $T_N = 120°C$, $R_N = 3$, 5, and 7 billets were drawn up to 500 mm min^{-1} without fracture (Fig. 3c), the maximum draw ratios being 8.0, 12.5, and 17.6, respectively. Billets of $R_N = 9$ were also drawn at up to 500 mm min^{-1}, although there was no improvement in the surface disruption that had been observed at 110°C. However, no crossover occurred in the R_A versus V_f curves for $R_N = 7$ and 9 billets, as the R_A values for the $R_N = 7$ products dropped owing to increase in temperature. The R_A values were low for $R_N = 9$ billets products, again probably due to overestimates of disrupted surface product diameters. It was not possible to draw $R_N = 11$ billets at this temperature since early fracture was observed at the start-up phase.

At $T_N = 155°C$ (Fig. 3d), $R_N = 3$, 5, 7, and 9 billets were drawn at speeds up to 500 mm min^{-1}, the maximum draw ratios obtained being 7.1, 9.1, 12.7, and 21.5, respectively. Smooth-surfaced products for $R_N = 9$ were obtained at this temperature. Billets of $R_N = 11$ were drawn up to speeds of 100 mm min^{-1} beyond which fracture occurred, the maximum draw ratio obtained being 17.2. Stable die drawing of $R_N = 13$ billets at 155°C was not possible.

Higher drawing temperatures were not used because of the proximity to the melting point (164°C) of the material.

It can be observed from Figure 3 that with increasing draw temperature the slopes of the R_A versus V_F curves decreased for a given billet size.

It was considered of interest to extend the drawing of $R_N = 9$ billets to other temperatures between 120 and 155°C; therefore, billets were also drawn at 140 and 150°C. Drawing was carried out to give smooth-surfaced products at $T_N = 140°C$ up to a draw speed of 200 mm min^{-1}, beyond which fracture occurred (Figure 4). A maximum draw ratio of 23.2 at 200 mm min^{-1} was obtained, which was also the maximum draw ratio obtained in this work. At

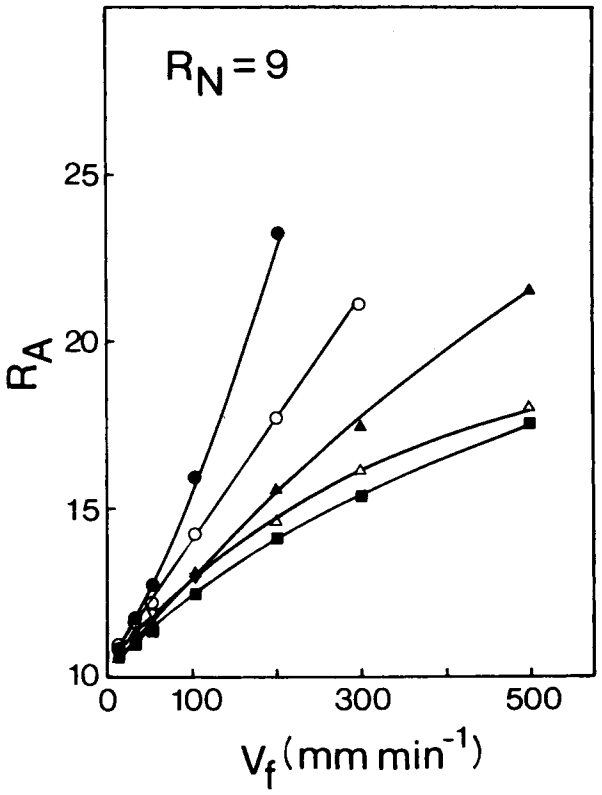

Fig. 4. Variation of draw ratio R_A with draw speed V_f, for $R_N = 9$ billets, draw temperatures as indicated: ■ $T_N = 110°C$; △ $T_N = 120°C$; ● $T_N = 140°C$; ○ $T_N = 150°C$; ▲ $T_N = 155°C$.

$T_N = 150°C$ it was possible to increase the draw speed up to 300 mm min^{-1} for $R_N = 9$ billets but the maximum draw ratio dropped to 21.2. Figure 4 also includes the results for this billet size at $T_N = 110$, 120, and 155°C. For $R_N = 11$ billets at $T_N = 150°C$, surface peeling of the drawn products was observed even at the low draw speed of 10 mm min^{-1}. Surface material appeared to be scraped away within the die, which led to failure at the die exit. It appears that a drawing temperature of 155°C is the minimum for billets of $R_N = 11$.

The variation of steady draw load with imposed draw speed is shown in Figure 5. After an initial region of increasing load with V_f, the slopes decrease drastically for all R_N and T_N values. Draw load is determined by the work done per unit volume in the material passing through the die flow zone. Essentially, an increase in draw speed increases the load because of the strain rate dependence of the flow stress of the material, and therefore the work done per unit volume increases. The heat of deformation increases with increasing draw speed, which may cause the decrease in the slopes of L versus V_f curves. The draw loads were substantially reduced at all speeds for given billet sizes with increasing draw temperature, reflecting a decrease in material flow stress.

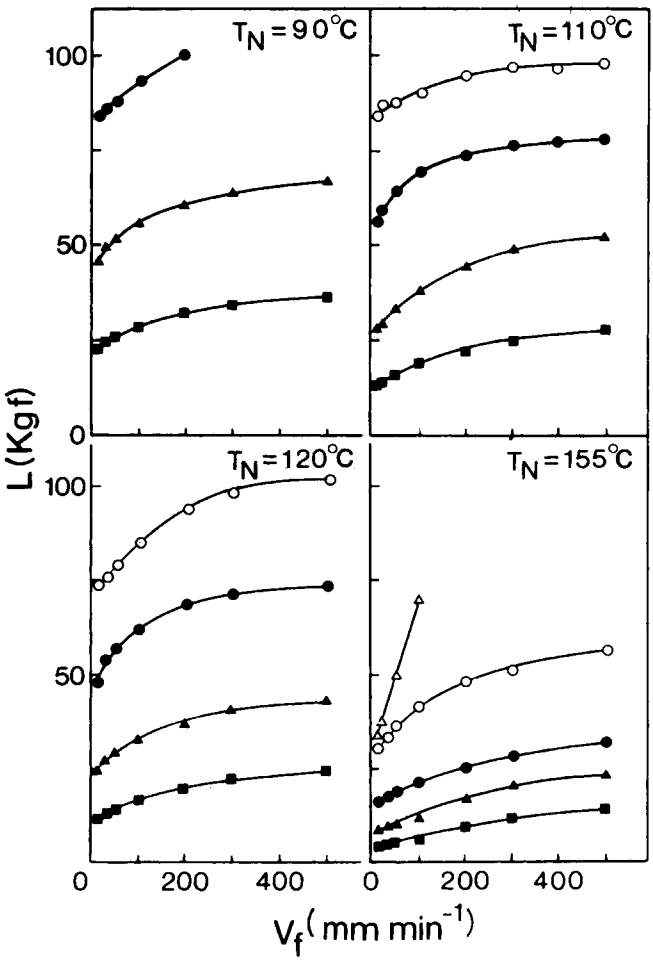

Fig. 5. Variation of draw load L with draw speed V_f, draw temperatures as indicated: ■ $R_N = 3$; ▲ $R_N = 5$; ● $R_N = 7$; ○ $R_N = 9$; △ $R_N = 11$.

The variation of maximum draw stress σ_{max} with draw speed for different R_N and T_N values is shown in Figure 6. It can be seen that σ_{max} rises with increasing draw speed for all R_N billets at each draw temperature. These draw stresses fell substantially with increasing draw temperature.

The variation of maximum draw stress σ_{max} with draw speed for $R_N = 9$ billets at different draw temperatures is shown in Figure 7. It can be observed that, for drawing of smooth-surfaced products at $T_N \geq 140°C$, the draw stress increases very rapidly as the draw temperature decreases. It is apparent that at $T_N = 110$ and 120°C the σ_{max} values should be substantially greater than the actual levels. At these temperatures, initial high draw stresses at low draw speeds initiate tearing and disruption of the surface of the drawn product; perceived stresses at higher speeds then fall off, as shown in the Figure 7. Surface disruption of these products gave excessive apparent diameters, leading to overestimated cross-sectional areas that reduced the calculated values of σ_{max}.

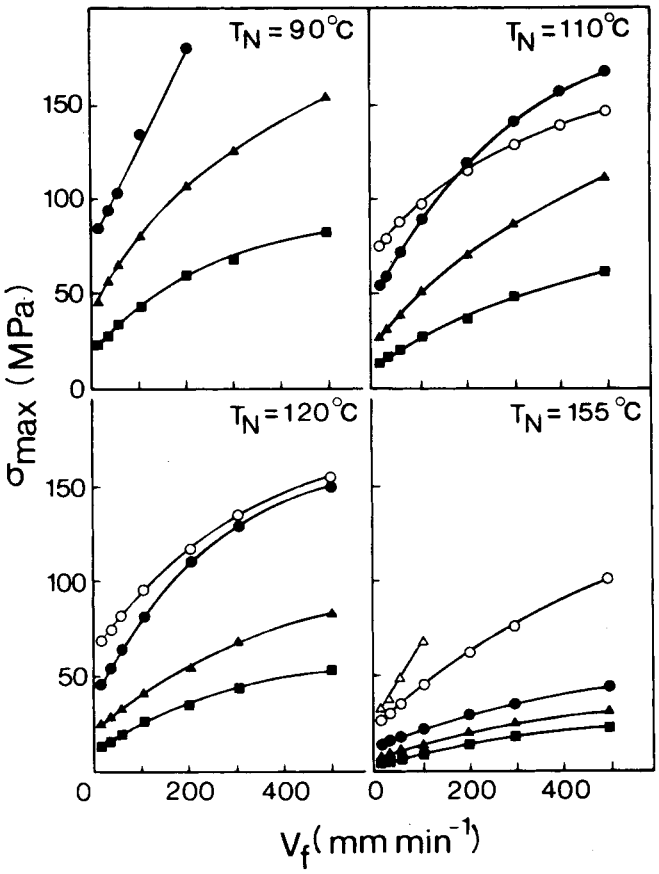

Fig. 6. Variation of draw stress σ_{max} with draw speed V_f, draw temperatures as indicated: ■ $R_N = 3$; ▲ $R_N = 5$; ● $R_N = 7$; ○ $R_N = 9$; △ $R_N = 11$.

It was observed that the nonisothermal postdie drawing in zone 3 increased with increasing draw temperatures and speeds. It is probable that increased heat carryover into zone 3 in these situations allows a greater amount of drawing to occur there. Figure 8 shows the necking profile for $R_N = 7$ billets drawn at 110°C. The left-hand side sample was drawn at 10 mm min^{-1} to $R_A = 8.6$, and the right-hand side sample was drawn at 300 mm min^{-1} to $R_A = 16.7$. The effect of the higher drawing speed on zone 3 is clear, with a significant increase in the drawing that occurs there.

Visual examination of the drawn products showed that at low draw speeds transparency increased with increasing R_N value and draw temperature. It was observed, however, that transparency depends on the draw stress σ_{max} applied during drawing. Transparency of the product persisted up to a critical stress level σ_{max} of about 100 MPa at all draw temperatures; this is indicated in Figure 9, which gives σ_{max} against R_A. Above this critical stress value the product became increasingly stress whitened, possibly due to the formation of microvoids. The maximum R_A values up to which products remain transparent increases with increasing draw temperature; for draw temperatures 90,

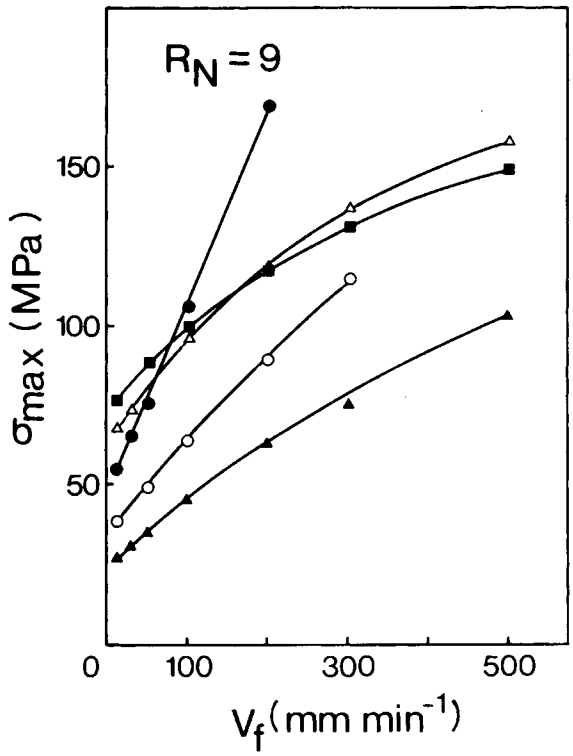

Fig. 7. Variation of draw stress σ_{max} with draw speed V_f, for $R_N = 9$ billets: ■ $T_N = 110°C$; △ $T_N = 120°C$; ● $T_N = 140°C$; ○ $T_N = 150°C$; ▲ $T_N = 155°C$.

110, 120, and 155°C these R_A values are about 10.5, 12.5, 13.0, and 20.0, respectively.

Samples cut from the core of products of $R_A = 8.6$ and 17.5 drawn at 110°C, at draw speeds of 10 and 500 mm min^{-1}, respectively, were examined by scanning electron microscopy (SEM). The stress levels during die drawing for these samples had been 53 and 150 MPa, respectively, that is, below and above the critical stress whitening level. Substantial microvoiding was observed in the SEM examination of the sample of $R_A = 17.5$. The presence and formation of microvoids in die-drawn products of POM have been discussed in detail by Hope et al.,[22] who found that microvoid formation occurred during the free drawing part of the process (in zone 3) at moderate draw ratios.

Figure 9 also demonstrates that at each drawing temperature a unique and substantially straight-line relationship for σ_{max} versus R_A was apparent; no difference in each relationship appeared for diverging routes to a given draw ratio, that is, for differing R_N and V_f combinations.

The visual quality of the products was good for all R_N, V_f, and T_N values, except for the $R_N = 9$ products at 110 and 120°C, where surface disruption occurred. There was very little fluctuation in product diameter at steady-state drawing, and diameter at a given draw temperature, speed, and billet R_N was reproducible.

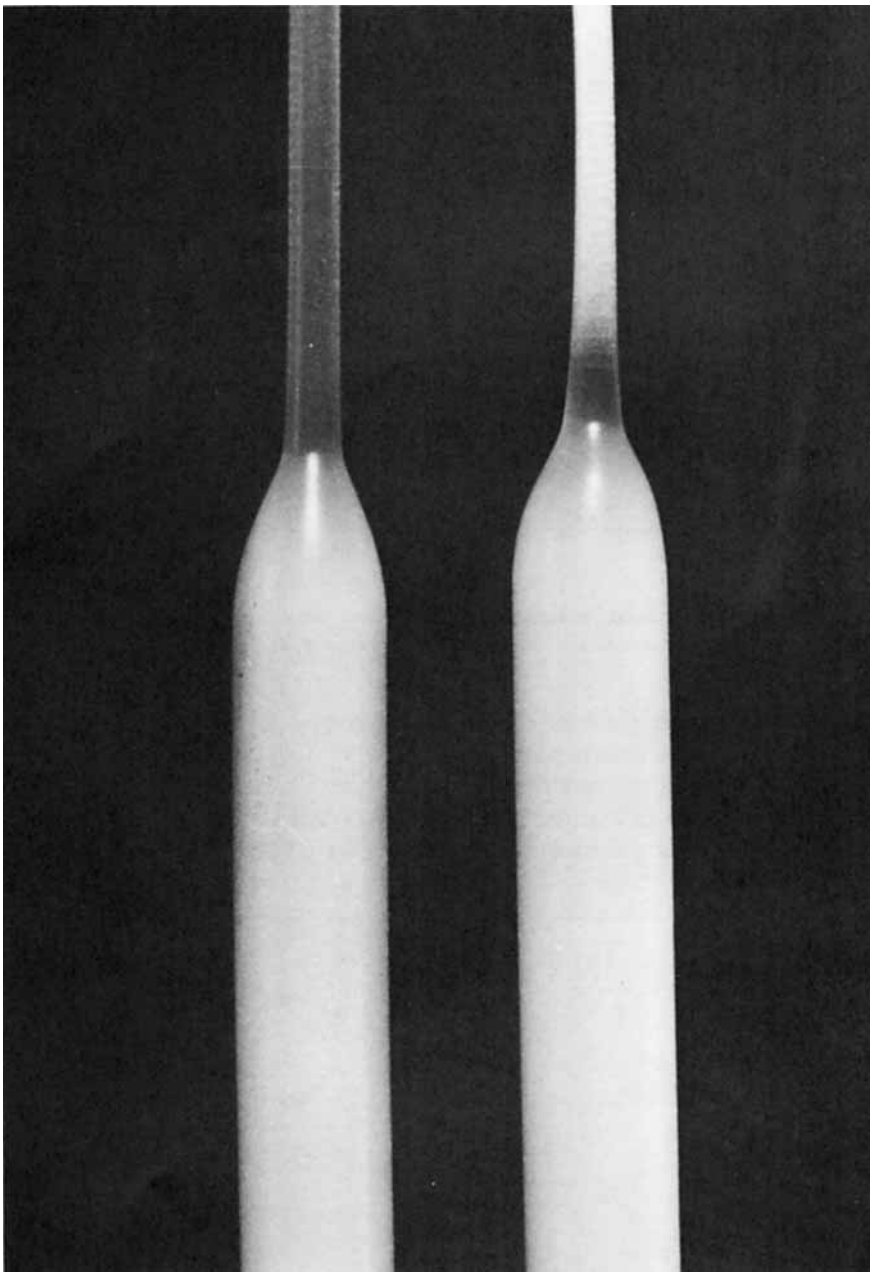

Fig. 8. Necking profiles for $R_N = 7$ billets drawn at 110°C. Left-hand side sample, $V_f = 10$ mm min^{-1}, R_A 8.6; Right-hand side sample, $V_f = 300$ mm min^{-1}, $R_A = 16.7$.

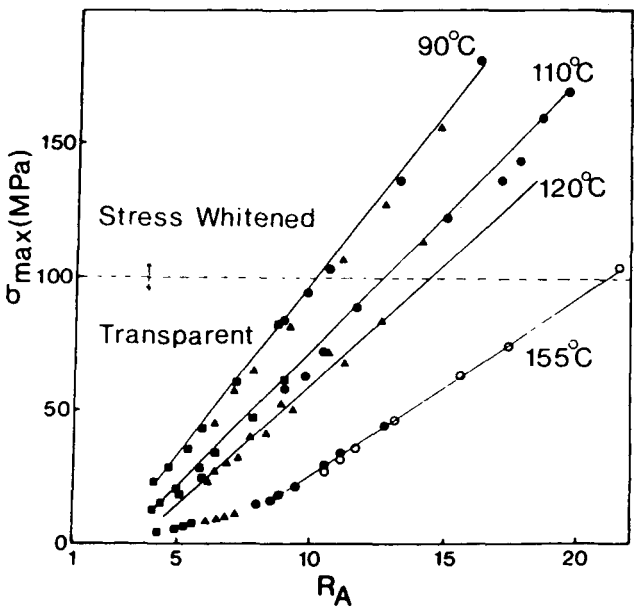

Fig. 9. Variation of visual appearance of the products and draw stress σ_{max} with draw ratio R_A, draw temperatures as indicated: ■ $R_N = 3$; ▲ $R_N = 5$; ● $R_N = 7$; ○ $R_N = 9$.

Turning to higher speed die drawing using the large-scale machine, billets of $R_N = 5$ and 7 were drawn without fracture at $T_N = 155$°C up to the maximum draw speed of the machine (2000 mm min^{-1}). The R_A values are shown against draw speed in Figure 10. The previous data points obtained using the small-scale drawing machine are superimposed on this figure up to a draw

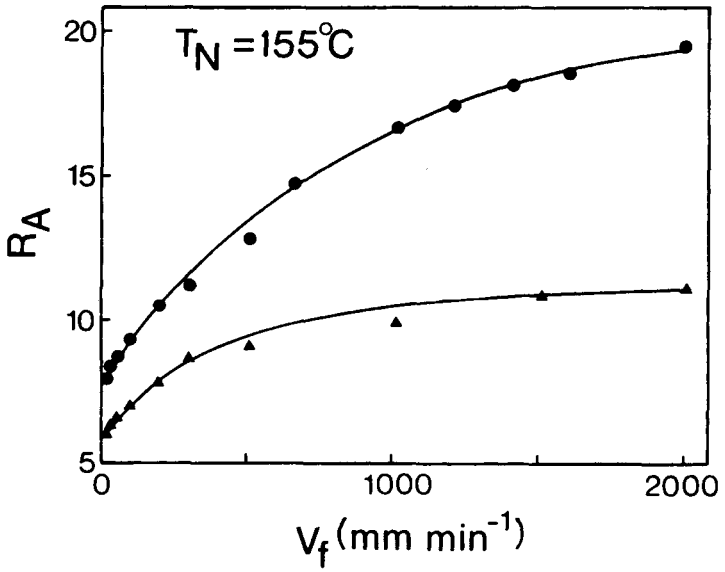

Fig. 10. Variation of draw ratio R_A with draw speed V_f, at a draw temperature of 155°C: ▲ $R_N = 5$; ● $R_N = 7$.

speed of 500 mm min^{-1}, the large-scale machine being used at between 650 and 2000 mm min^{-1}. No accurate load measurement was possible because of comparative insensitivity of the load cell on the large-scale machine (which was designed primarily for drawing large sections); therefore no drawing stress levels are presented. Maximum draw ratios of 11.3 and 19.3 were achieved for $R_N = 5$ and 7 billets, respectively. It was noted that the zone 3 necking extended remarkably at these higher speeds, reaching about 15 cm beyond the die at $V_f = 2000$ mm min^{-1}.

It is of considerable commercial interest to die draw enhanced modulus products at high speeds in order to achieve economical production.

Mechanical Properties

The 10 s Young's modulus E at 20°C for the die-drawn products from different R_N billets drawn at 110 and 155°C are shown in Figures 11 and 12, respectively. In both cases the modulus of the products increases in a substantially linear manner with draw ratio. The maximum modulus at 110°C draw temperature was 16.5 GPa for $R_A = 19.5$. A modulus of 18.4 GPa was recorded for $R_A = 21.5$ drawn at 155°C.

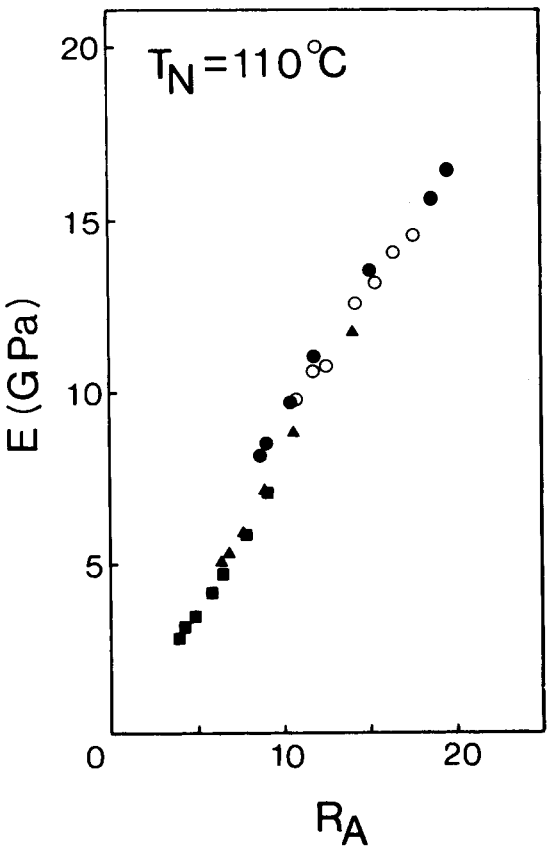

Fig. 11. Variation of product three-point bend modulus E with draw ratio R_A, draw temperature = 110°C: ■ $R_N = 3$; ▲ $R_N = 5$; ● $R_N = 7$; ○ $R_N = 9$.

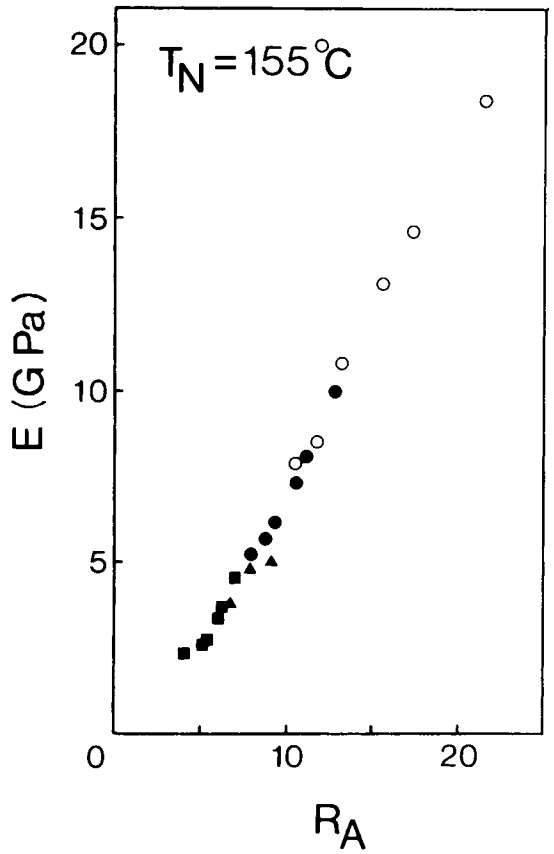

Fig. 12. Variation of product three-point bend modulus E with draw ratio R_A, draw temperature = 155°C: ■ $R_N = 3$; ▲ $R_N = 5$; ● $R_N = 7$: ○ $R_N = 9$.

The effect of drawing temperature on modulus E of the $R_N = 7$ products is shown in Figure 13. It was observed that as the draw temperature increases the modulus drops significantly for the products obtained at lower draw speeds, that is, at lower draw ratios. The effect of draw temperature on modulus reduces to some extent at high R_A values, that is, for the products drawn at higher speeds. The drop in modulus of the product drawn at 90°C at high speed ($R_A = 16.2$) may be due to the presence of heavy voiding, which was apparent in the sample. Figure 14 shows E values for all the samples measured in this work, at all R_N values, temperatures, and speeds; the modulus shows a substantially linear relationship with draw ratio for all R_N and draw temperature values. It was observed that considerable postdie drawing in zone 3 took place at higher draw speeds and that this effect increased with increasing draw temperature. It appears that this nonisothermal drawing in zone 3 may counteract the lowering effect of high die temperature on modulus, since the high strain element of the deformation then occurs in a cooling zone. In the case of LPE, Gibson and Ward[20] have pointed out that the moduli obtained from die drawing are likely to depend

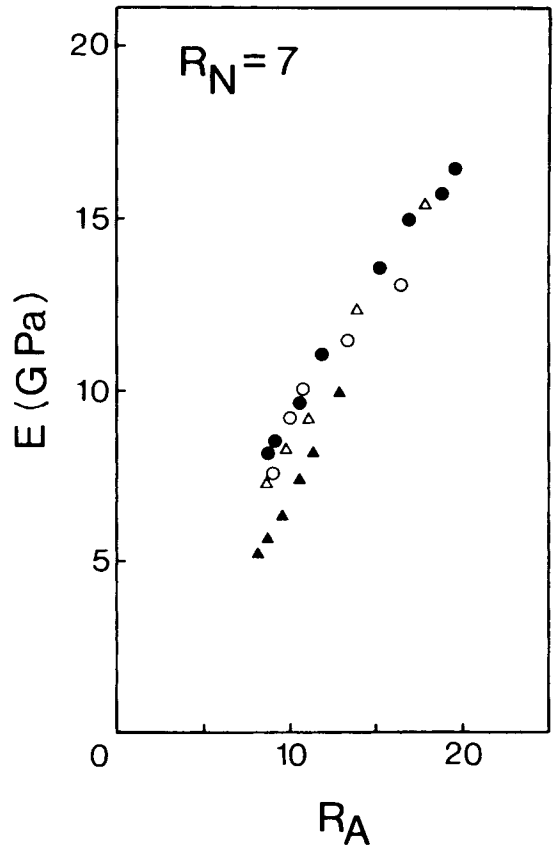

Fig. 13. Variation of product three-point bend modulus E with draw ratio R_A at various draw temperatures, billet $R_N = 7$: ○ $T = 90°C$; ● $T_N = 110°C$; △ $T_N = 120°C$; ▲ $T_N = 155°C$.

strongly on the thermal and strain rate paths followed by the material after leaving the die.

A maximum modulus of 20 GPa was achieved; this was for the product drawn to $R_A = 23.2$ from a billet of $R_N = 9$ at 140°C. This compares with a three-point bending modulus value of 1.5 GPa obtained for an isotropic rod machined from GSE 108 polypropylene bar stock.

The product drawn to $R_A = 19.3$ at the speed of 2000 mm min^{-1} at $T_N = 155°C$ had a modulus of 16.5 GPa.

Figure 15 shows the relationship between modulus and drawing stress σ_{max} for draw temperatures of 110 and 155°C. It is observed that this relationship depends on draw temperature. At the higher draw temperature stresses are lower for the same modulus value. Similar behavior has been observed for the tensile drawing of PVDF.[30]

The modulus results of the products drawn at 110 and 155°C at higher speeds ($\geq$ 300 mm min^{-1}) lie on the same modulus-draw ratio curve (Fig. 14), but the higher draw temperature allows a greater modulus for the same σ_{max} (Fig. 15). This must be due to some advantageous balance of draw tempera-

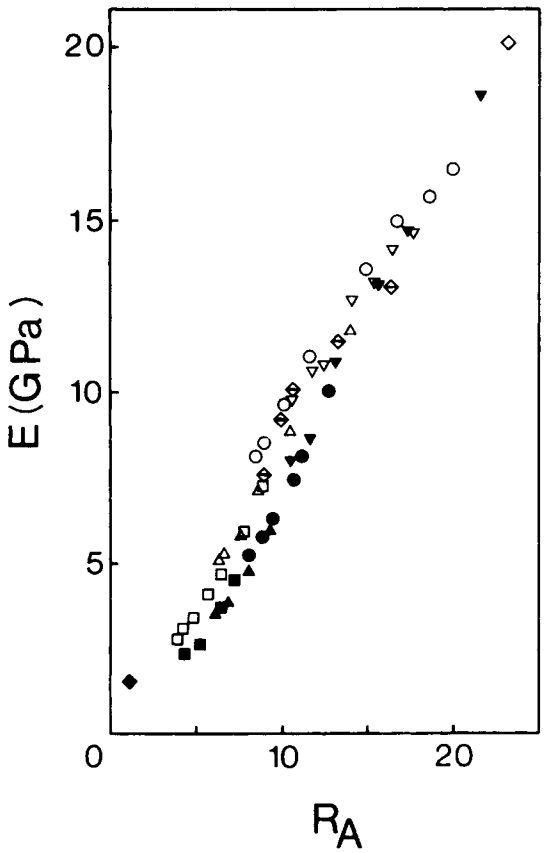

Fig. 14. Variation of product three-point bend modulus E with draw ratio R_A for various draw temperatures: ◆ isotropic; $R_N = 3$ (■ $T_N = 155°C$, □ $T_N = 110°C$); $R_N = 5$ (▲ 155°C, △ 110°C); $R_N = 7$ (● 155°C, ○ 110°C, ◈ 90°C); $R_N = 9$; (▼ 155°C, ▽ 110°C, ◇ 140°C).

ture, draw speed, and nonisothermal postdie drawing, the details of which are at present unresolved.

Figure 16 shows the temperature dependence of $\tan\delta$ for samples of different draw ratios produced at 110°C. The $\tan\delta$ peak located at about 5°C corresponds to the β relaxation. This β relaxation is known to be associated with glass-transition initiation of micro-Brownian motion in amorphous chains.[31] It is observed that the intensity of this peak reduces progressively with increasing draw ratio and disappears in the sample of $R_A = 18.2$. This reduction and disappearance of the β-relaxation peak may be ascribed to an increased number of taut-tie molecules with increasing draw ratio, which hardly engage in micro-Brownian motion. This β relaxation reappears in a sample of $R_A = 18.2$, which is freely annealed at 145°C (Fig. 17), where it may be considered that the taut-tie molecules relax during annealing. A small peak at $-55°C$ in the isotropic sample is also observed in Figure 16; Takayanagi et al.[31] reported that a secondary loss appears at about $-70°C$ as a shoulder in the general curve. The absolute loss level is anomalously high for the sample of $R_A = 18.2$ below room temperature; this may be an artefact due to

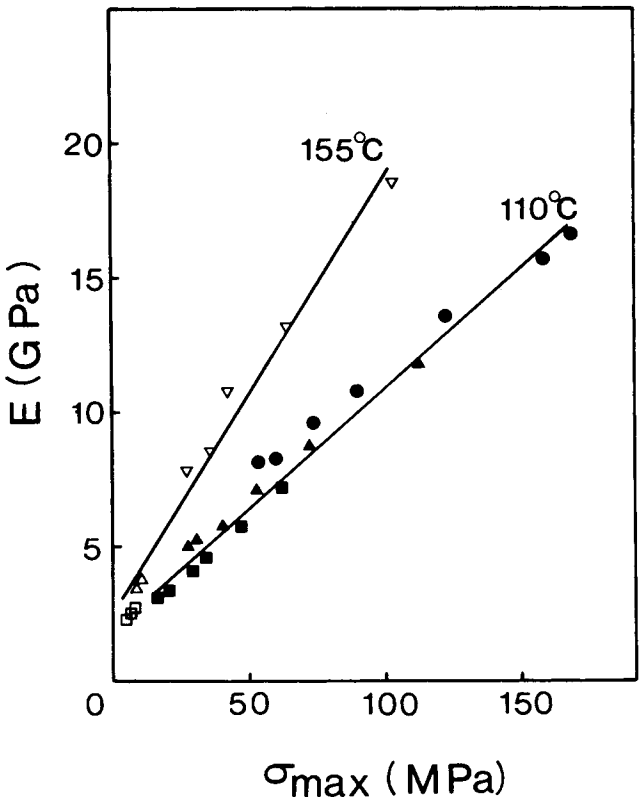

Fig. 15. Variation of product three-point bend modulus E with draw stress σ_{max} for draw temperatures 110 and 155°C: ■,□ $R_N = 3$; ▲,△ $R_N = 5$; ●,○ $R_N = 7$; ▽ $R_N = 9$.

the heavy voiding that was apparent in the sample.

Figure 18 shows the temperature dependence of E' for the same samples. It is observed that E' increases with increasing draw ratio over all ranges of temperature. Figure 19 shows that the E' drops substantially at all temperatures following the free annealing treatment of the $R_A = 18.2$ sample.

A maximum dynamic modulus of 22 GPa was achieved at −80°C for the sample of $R_A = 18.2$ (which had a room temperature static three-point bend modulus of 16.5 GPa), which is equal to 52% of the theoretical crystal modulus.[32]

The dynamic mechanical behavior of the isotropic and drawn products are similar to those observed earlier in several investigations for isotropic and oriented polypropylene in various physical forms.[31,33-36]

The enhancement of modulus with drawing can be interpreted in terms of morphological changes produced during orientation. According to Peterlin,[37] the strongest element of the oriented polymer is the microfibril. Each microfibril consists of crystalline chain-folded blocks alternating with amorphous layers with many axial tie molecules. As the draw ratio increases, the fraction of tie molecules increases as a result of the chain unfolding, and this enhances the axial elastic modulus of the drawn product.

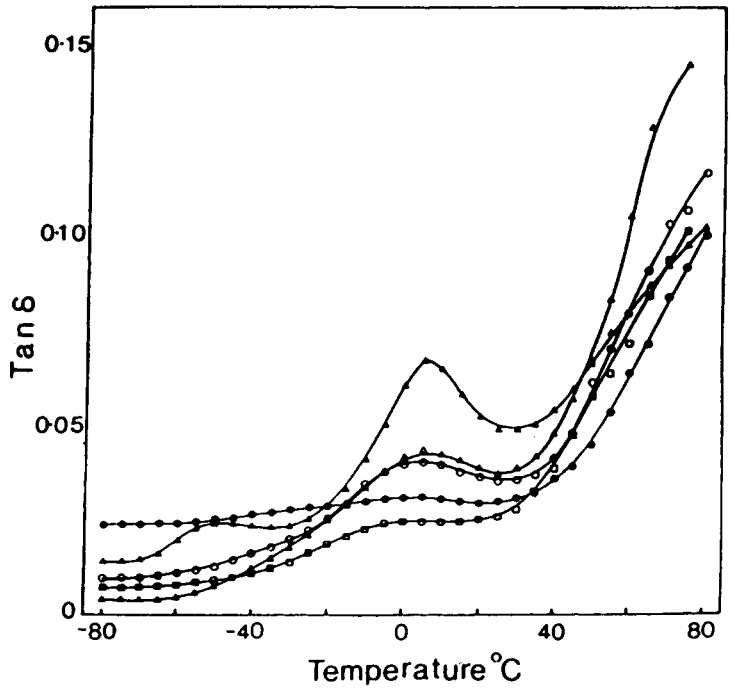

Fig. 16. Temperature dependence of dynamic loss tan δ, draw temperature = 110°C: ▲ isotropic; △ R_A = 4.2; ○ R_A = 6.3; □ R_A = 10.3; ● R_A = 18.2.

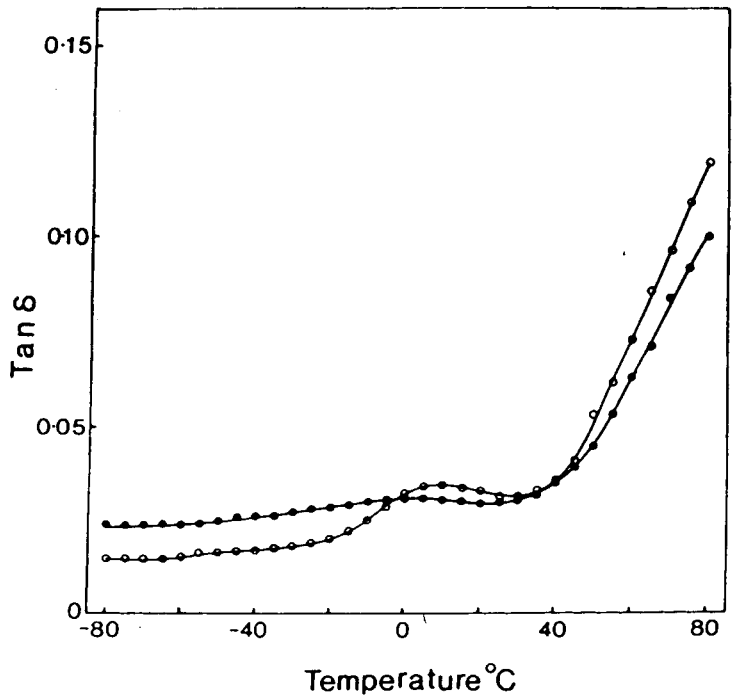

Fig. 17. Temperature dependence of dynamic loss tan δ: ● R_A = 18.2; ○ R_A = 18.2, annealed freely at 145°C. Draw temperature = 110°C.

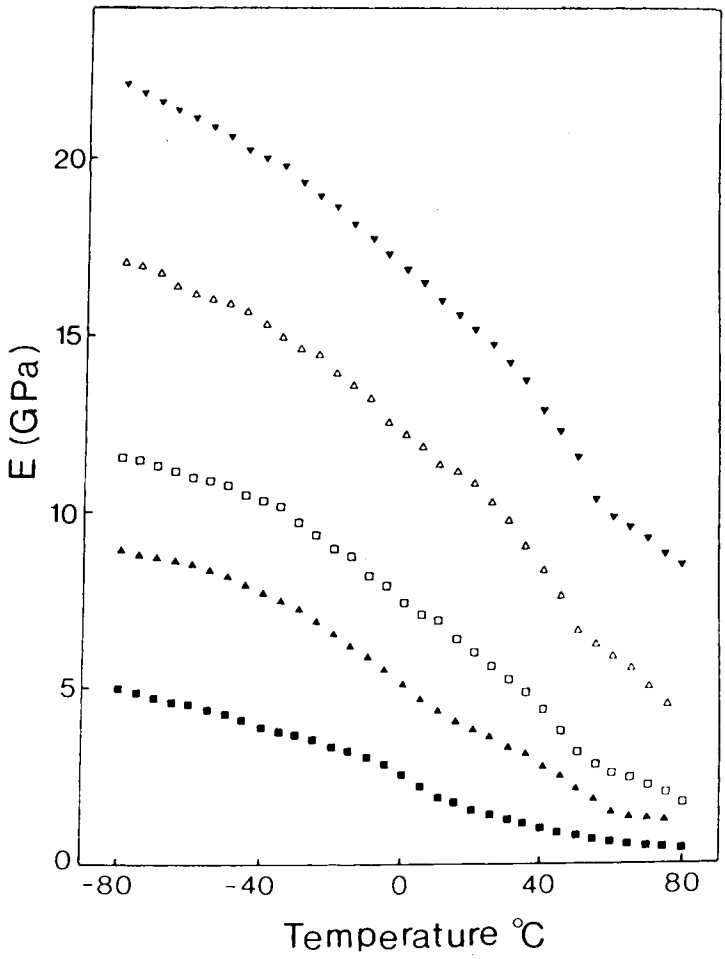

Fig. 18. Temperature dependence of dynamic modulus E'. Draw temperature = 110°C: ■ isotropic; ▲ R_A = 4.2; □ R_A = 6.3; △ R_A = 10.3; ▼ R_A = 18.2.

CONCLUSIONS

The production of oriented polypropylene rods has been studied comprehensively using the die drawing process. Draw ratios up to 23.2 were obtained giving room temperature static three-point bend moduli up to 20 GPa in the draw direction, which represents a substantial enhancement over the isotropic value of 1.5 GPa. It was found possible to produce the drawn products at speeds up to 2000 mm min^{-1} using a large-scale die drawing machine at a draw temperature of 155°C, giving draw ratios up to 19.3. Die drawing at speeds greater than 500 mm min^{-1} could not be studied comprehensively, the current billet-making technique not being sufficiently developed at the time of this work to produce very long, small-diameter billets. The draw ratio versus haul-off speed behavior for $R_N = 5$ and 7 at $T_N = 110$°C is similar to that obtained by Coates and Ward[19] at these R_N ratios using 15.5 and 7.0 mm exit diameter dies, but the present modulus values are slightly lower at high draw ratios.

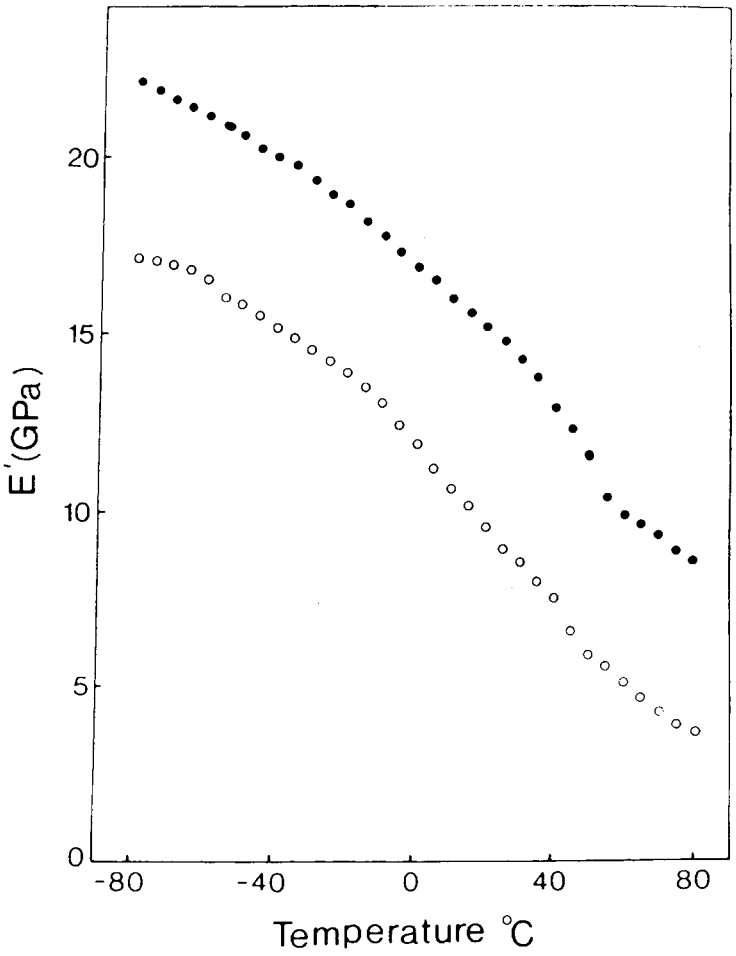

Fig. 19. Temperature depdendence of dynamic modulus E': ● R_A = 18.2; ○ R_A = 18.2, annealed freely at 145°C. Draw temperature = 110°C.

Transparency of the drawn rods increased with increasing billet R_N size and draw temperature, subject to a critical draw stress level of about 100 MPa. Above this critical stress level the material became increasingly stress whitened. Suitable conditions to make clear and very stiff material of commercial interest (perhaps in packaging applications) may therefore be defined in combinations of draw temperature, draw speed, and draw stress. For example, from Figures 3, 9, and 12 suitable conditions for die drawing a clear, high-R_A, and high-modulus product from this grade of polypropylene are as follows (draw temperature = 155°C):

$$R_N = 9$$

$$R_A = 16\text{–}20$$

$$V_f = 220\text{–}400 \text{ mm min}^{-1}$$

$$\sigma_{max} = 65\text{–}90 \text{ MPa}$$

$$E = 13\text{–}17 \text{ GPa}$$

The relative enhancement of modulus with draw ratio was seen to be retained over the temperature range of dynamic mechanical testing, from −80 to +80°C. Further work is to be reported involving structural analysis of these samples using differential scanning calorimetry, wide-angle x-ray scattering, and birefringence measurements. The die drawing process is potentially continuous, and current work in this laboratory is directed to the development of a practical continuous process for the commercial die drawing of highly oriented polymers.

References

1. G. Capaccio, T. A. Crompton, and I. M. Ward, *J. Polym. Sci., Polym. Phys. Ed.*, **14**, 1641 (1976).
2. G. Capaccio, T. A. Crompton, and I. M. Ward, *J. Polym. Sci., Polym. Phys. Ed.*, **18**, 301 (1980).
3. D. L. M. Cansfield, G. Capaccio, and I. M. Ward, *Polym. Eng. Sci.*, **16**, 721 (1976).
4. A. J. Wills, G. Capaccio, and I. M. Ward, *J. Polym. Sci., Polym. Phys. Ed.*, **18**, 493 (1980).
5. B. Brew and I. M. Ward, *Polymer*, **19**, 1338 (1978).
6. A. G. Gibson and I. M. Ward, *J. Polym. Sci., Polym. Phys. Ed.*, **16**, 2015 (1978).
7. P. S. Hope, A. G. Gibson, B. Parsons, and I. M. Ward, *Polym. Eng. Sci.*, **20**, 540 (1980).
8. P. S. Hope and B. Parsons, *Polym. Eng. Sci.*, **20**, 589 (1980).
9. P. S. Hope and B. Parsons, *Polym. Eng. Sci.*, **20**, 597 (1980).
10. P. S. Hope, A. G. Gibson, and I. M. Ward, *J. Polym. Sci., Polym. Phys. Ed.*, **18**, 1243 (1980).
11. T. Williams, *J. Mater. Sci.*, **8**, 59 (1973).
12. P. D. Coates and I. M. Ward, *J. Polym. Sci., Polym. Phys. Ed.*, **16**, 2031 (1978).
13. K. Nakamura, K. Imada, and M. Takayanagi, *Int. J. Polym. Mater.*, **2**, 71 (1972).
14. K. Imada and M. Takayanagi, *Int. J. Polym. Mater.*, **2**, 89 (1972).
15. S. Maruyama, K. Imada, and M. Takayangi, *Int. J. Polym. Mater.*, **2**, 105 (1973).
16. S. Maruyama, K. Imada, and M. Takayangi, *Int. J. Polym. Mater.*, **2**, 125 (1973).
17. N. J. Capiati, S. Kojima, W. G. Perkins, and R. S. Porter, *J. Mater. Sci.*, **13**, 334 (1977).
18. A. E. Zachariades, W. T. Mead, and R. S. Porter, in *Ultra-High Modulus Polymers*, A. Ciferri and I. M. Ward, Eds., Applied Science Publishers, London, 1979, Chapter 2.
19. P. D. Coates and I. M. Ward, *Polymer*, **20**, 1553 (1979).
20. A. G. Gibson and I. M. Ward, *J. Mater. Sci.*, **15**, 979 (1980).
21. A. G. Gibson and I. M. Ward, *Polym. Eng. Sci.*, **20**, 1229 (1980).
22. P. S. Hope, A. Richardson, and I. M. Ward, *J. Appl. Polym. Sci.*, **26**, 2879 (1981).
23. P. S. Hope, A. Richardson, and I. M. Ward, *Polym. Eng. Sci.*, **22**, 307 (1982).
24. A. Richardson, P. S. Hope, and I. M. Ward, *J. Polym. Sci., Polym. Phys. Ed.*, **21**, 2525 (1983).
25. A. Richardson, F. Ania, D. R. Rueda, I. M. Ward, and F. J. Baltá-Calleja, *Polym. Eng. Sci.*, **25**, 355 (1985).
26. I. M. Ward, A. Selwood, B. Parsons, and A. Gray, Plastic Pipes VI, University of York, March 26–28, 1985.
27. B. Parsons, A. Selwood, and I. M. Ward, *Plastics and Rubber Processing and Applications*, to be published.
28. A. Richardson, B. Parsons, and I. M. Ward, Plastics and Rubber Processing and Applications, to be published.
29. A. G. Gibson, Ph.D. Thesis, University of Leeds, 1977.
30. J. Humphreys, private communication.
31. M. Takayangi, K. Imada, and T. Kajiyama, *J. Polym. Sci.*, C, **15**, 263 (1966).
32. I. Sakurada, T. Ito, and K. Nakamae, *J. Polym. Sci.*, C, **15**, 75 (1966).
33. A. J. Owen and I. M. Ward, *J. Macromol. Sci. Phys.*, **B7**(3), 417 (1973).
34. J. Petermann and J. M. Schultz, *J. Mater. Sci.*, **13**, 2188 (1978).
35. S. Nagon and K. Azuma, *J. Macromol. Sci., Phys.*, **B16**(3), 435 (1979).
36. S. Nagon and S. Oba, *J. Macromol. Sci.*, **B18**(2), 281 (1980).
37. A. Peterlin, *J. Mater. Sci.*, **6**, 490 (1971).

Received May 1, 1986
Accepted August 11, 1986